E-proceedings of the 36th IAHR World Congress
28 June – 3 July, 2015, The Hague, the Netherlands

LONG WAVES IN CURVED AND BRANCHING CHANNELS OF ARBITRARY CROSS-SECTION

PATRICIO WINCKLER GREZ[(1)] & PHILIP L.-F. LIU[(2),(3)]

[(1)] *Universidad De Valparaíso, Valparaíso, Chile,*
patricio.winckler@uv.cl

[(2)] *Cornell University, Ithaca, United States*

[(3)] *National Central University, Taiwan*

pll3@cornell.edu

ABSTRACT

A series of 1D cross-sectional averaged theories of long waves in channels have been developed (e.g. Peregrine, 1968; Teng & Wu, 1997). However, none of them is able to account simultaneously for i) arbitrary and asymmetric cross-sections with respect to the direction of wave propagation, ii) channel cross-sections that can change appreciatively within a wavelength, iii) curvature in the horizontal plane, iv) branching and v) viscous dissipation from the bottom boundary layer. In natural streams, however, riverbanks are not straight, channels can often have bends or branches and the cross-section may be highly non-uniform. Examples of such are found in tsunami waves traveling along rivers, ocean tides in fjord systems or storm surge entering harbors. In this paper we summarize part of the authors' work (Winckler, 2015; Winckler & Liu, 2015) to account for some of these phenomena.

Keywords: *Boussinesq waves, curved channels, branching channels, viscous dissipation*

1. LONG WAVE EQUATIONS FOR A CURVED CHANNEL

A generalization of the cross-sectional averaged 1D long wave model for straight channels derived by Winckler and Liu (2015) is proposed herein to account for curvature in the horizontal plane. The derivation is based on a specific set of orthogonal curvilinear coordinates, arbitrarily defined from one of the channel's sidewalls. 3D equations of motion for inviscid and incompressible fluid in this curvilinear coordinate system are integrated over a channel cross-section. After invoking a perturbation expansion, the resulting 1D equations are expressed in terms of the cross-sectional quantities. The new equations are of the Boussinesq form, implying that frequency dispersion is small but not negligible, and balanced by nonlinearity. The equations explicitly contain the curvature and reduce to governing equations for straight channels derived by Winckler and Liu (2015).

The main geometrical assumptions are i) that the local radius of curvature is much larger than the characteristic wavelength, ii) the characteristic depth and width of the channel cross-section are assumed to be smaller than the typical wavelength, iii) the sidewall slope at the still water level is order $O(1)$ and iv) changes in the geometry along the channel can change significantly within a wavelength.

Consider a channel of arbitrary cross-section with a specific curvilinear coordinate system $(\hat{s},\hat{\sigma},\hat{z})$ depicted in Figure 1. Here $\hat{s}$ is the arclength measured along the right sidewall at still water level, $\hat{\sigma}$ denotes the distance measured orthogonally into the flow domain and $\hat{z}$ is the vertical coordinate pointing upwards; $\hat{z}=0$ denotes the still water level (SWL). Hats represent dimensional variables. The $\hat{s}$-axis is required to be continuous and smooth and the channel is curved only on the horizontal $\hat{s}-\hat{\sigma}$ plane. The transformation between Cartesian coordinates $(\hat{x},\hat{y},\hat{z})$ and curvilinear orthogonal coordinates for an arbitrary point at the still water level within the fluid domain $P_1(\hat{s},\hat{\sigma},\hat{z}=0)$ is (Dressler, 1978)

$$\hat{x}(\hat{s},\hat{\sigma})=\hat{\xi}-\hat{\sigma}sin\theta, \qquad \hat{y}(\hat{s},\hat{\sigma})=\hat{\zeta}+\hat{\sigma}cos\theta \qquad [1]$$

where P is a point at $\hat{x}=\hat{\xi}(\hat{s})$, $\hat{y}=\hat{\zeta}(\hat{s})$ on the reference curve, $\theta(\hat{s})$ is the angle between $\hat{x}$ and the right sidewall, measured counterclockwise, The velocity $\hat{U}=(\hat{u},\hat{v},\hat{w})$ is defined by components in the longitudinal $\hat{s}$, spanwise $\hat{\sigma}$, and vertical direction $\hat{z}$, respectively. The curvature is defined by $\hat{\kappa}=d\theta/d\hat{s}$, where $\hat{\kappa}>0$ for concave channels and $\hat{\kappa}<0$ for convex channels.

The curvilinear coordinate system is required be one to one, implying every element $(\hat{x},\hat{y},\hat{z})$ corresponds to exactly one element of $(\hat{s},\hat{\sigma},\hat{z})$. For a convex channel with $\hat{\kappa}<0$, no restriction is required. For a concave channel with $\hat{\kappa}>0$ however, any point within the fluid domain needs the additional requirement of $\hat{\sigma}<\hat{R}$, where $\hat{R}$ is the radius of curvature. Thus, the channel width must be smaller than the radius of curvature, i.e. $\hat{B}_0<\hat{R}$, where $\hat{B}_0$ is the surface width of the channel at the quiescent state.

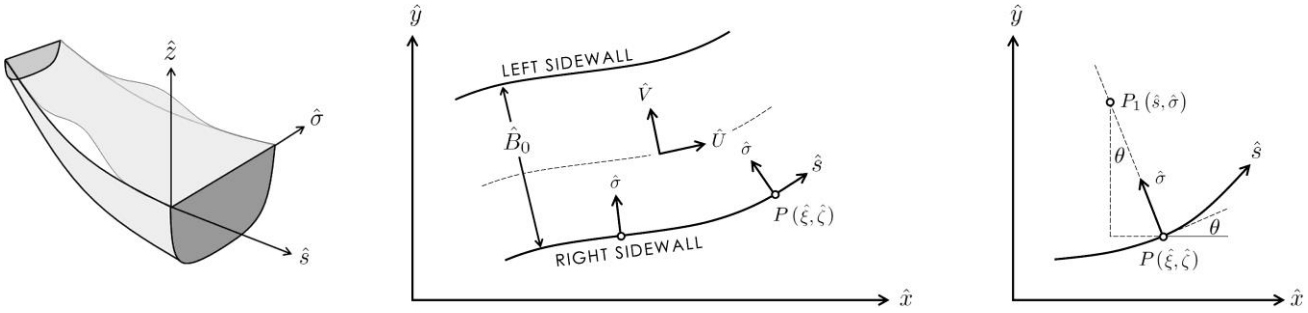

Figure 1. Curvilinear coordinate system used in the derivation of the theory.

To describe the problem in terms of dimensionless variables, the characteristic wavelength $\hat{\lambda}_0$ is employed as the length scale in the longitudinal direction, the characteristic unperturbed water depth $\hat{h}_0$ as the length scale for the vertical and spanwise directions, the typical wave amplitude $\hat{a}_0$ is used to account to effects of the free surface on the motion and $\hat{R}_0$ is the typical radius of curvature. The non-dimensional parameters

$$\mu = \hat{h}_0/\hat{\lambda}_0, \qquad \varepsilon = a_0/\hat{h}_0, \tag{2}$$

are introduced as measures of the frequency dispersion and nonlinearity, respectively. The Boussinesq approximation is assumed, thus $O(\varepsilon) = O(\mu^2) = 1$. The scalings used in Winckler and Liu (2015) are applied herein. The only new scaling is introduced for the curvature, $\hat{\kappa} = 1/\hat{R}$, as follows

$$\hat{\kappa} = \Upsilon\kappa/\hat{\lambda}_0, \tag{3}$$

where Υ accounts for the degree of curvature of the channel with respect to the wavelength. For $\Upsilon = \mu$ the radius of curvature is smaller than that for $\Upsilon = \varepsilon$; in both cases, however, the radius of curvature is smaller than the wavelength. Variables are scaled by different lengths scales, which are considered to follow the relations $\hat{R}_0 > \hat{\lambda}_0 > \hat{h}_0 > \hat{a}_0$.

The 3D flow problem is reduced to 1D by integrating the equations of continuity and conservation of momentum on the cross-sectional area. For the sake of brevity, the derivation is omitted herein but can be reviewed in Winckler (2015). The channel averaged conservation of mass, in dimensionless form, becomes

$$\left(1 - \Upsilon\mu\kappa\frac{B_0}{2}\right)\frac{\partial\tilde{\eta}}{\partial t} + \varepsilon\frac{B'_0}{B_0}\,\tilde{\eta}\frac{\partial}{\partial s}(A_0\langle u\rangle) + \frac{1}{B_0}\frac{\partial}{\partial s}([A_0 + \varepsilon B_0\tilde{\eta}]\langle u\rangle) - \Upsilon\mu\frac{\kappa}{B_0}\left(\vartheta\langle u\rangle + \Gamma\frac{\partial\langle u\rangle}{\partial s}\right) = O(\Upsilon\mu\varepsilon) \tag{4}$$

where $\tilde{\eta}$ is the spanwise averaged free surface elevation, $\langle u\rangle$ is the cross-sectional averaged longitudinal velocity,

$$A_0(s) = \int_0^{B_0} h(s,\sigma)d\sigma \tag{5}$$

is the cross-sectional area at the quiescent state, with h being the local depth, and B'_0 is the sidewall slope at the still water level. The coefficients ϑ and Γ stemming from the curvature are

$$\vartheta = \int_0^{B_0}\sigma\frac{\partial}{\partial\sigma}\left(h\frac{\partial\widetilde{\chi_1}}{\partial\sigma}\right)d\sigma + \int_0^{B_0}\sigma\frac{\partial\widetilde{\chi_1}}{\partial\sigma}d\sigma - h_{(B_0)}B_0\frac{\partial B_0}{\partial s} \tag{6}$$

and

$$\Gamma = \int_0^{B_0}\sigma\frac{\partial}{\partial\sigma}\left(h\frac{\partial\widetilde{\chi_2}}{\partial\sigma}\right)d\sigma + \int_0^{B_0}\sigma\frac{\partial\widetilde{\chi_2}}{\partial\sigma}d\sigma \tag{7}$$

where χ_1 and χ_2 are obtained from boundary value problems for each cross-section (equations 3.27 to 3.33 in Winckler and Liu's, replacing x by s). The symbol $\breve{f}$ represents the depth averaging of any function f. Note that for uniform symmetric channels, $\vartheta = \Gamma = 0$.

The channel averaged equation of conservation of momentum is

$$(1+\mu^2\alpha-\Upsilon\mu\kappa\sigma_c)\frac{\partial\langle u\rangle}{\partial t}+\frac{\partial\tilde{\eta}}{\partial s}+\varepsilon\langle u\rangle\frac{\partial\langle u\rangle}{\partial s}+\mu^2\beta\frac{\partial^2\langle u\rangle}{\partial t\partial s}+\mu^2\gamma\frac{\partial^3\langle u\rangle}{\partial t\partial s^2}=O(\Upsilon\mu\varepsilon) \quad [8]$$

where the term associated with α represents the correction to the local acceleration and the term associated with β denotes the wave decay or amplification caused by the variation of the cross-sectional geometry along the channel (Winckler and Liu, 2015). Both terms are negligible when the channel variations in the longitudinal direction become very small. The term associated with γ represents the frequency dispersion effects, which remain important even when the channel variations in the longitudinal direction are small. These coefficients are obtained once χ_1 and χ_2 are solved for each cross-section (equations 3.40 to 3.42 in Winckler and Liu's, replacing x by s).

In the authors' view, equations [4] and [8] provide a robust theory in a field where existing theories are heuristically derived (Fenton and Nadler, 1995) or applicable only to specific cases (Nachbim and da Silva, 2012). Fenton and Nadler (1995), for example, used a control volume approach without an explicit treatment of the kinematic and dynamic conditions at the free surface to derive a set of non-dispersive long wave equations for curved waterways. Nachbim and da Silva (2012), on the other hand, proposed a curvilinear Boussinesq model based on the technique of conformal mapping, to study the evolution of solitary waves on very specific geometries.

2. LONG WAVE EQUATIONS FOR A STRAIGHT CHANNEL

For a straight channel, the x by s coordinates coincide, thus equations [4] and [8] are simplified to

$$\frac{\partial\tilde{\eta}}{\partial t}+\varepsilon\frac{B'_0}{B_0}\tilde{\eta}\frac{\partial}{\partial x}(A_0\langle u\rangle)+\frac{1}{B_0}\frac{\partial}{\partial x}([A_0+\varepsilon B_0\tilde{\eta}]\langle u\rangle)=O(\varepsilon^2,\varepsilon\mu^2,\mu^4) \quad [9]$$

and

$$(1+\mu^2\alpha)\frac{\partial\langle u\rangle}{\partial t}+\frac{\partial\tilde{\eta}}{\partial x}+\varepsilon\langle u\rangle\frac{\partial\langle u\rangle}{\partial x}+\mu^2\beta\frac{\partial^2\langle u\rangle}{\partial t\partial x}+\mu^2\gamma\frac{\partial^3\langle u\rangle}{\partial t\partial x^2}=O(\varepsilon^2,\varepsilon\mu^2,\mu^4) \quad [10]$$

These equations coincide with those derived for a Cartesian coordinate system in Winckler and Liu (2015), in which the effects of rapid changes in the cross-sectional geometry occurring within a wavelength are included. These effects were not captured in earlier theories (e.g. Peregrine, 1968; Teng and Wu, 1997).

3. VISCOUS EFFECTS

Winckler (2015) extended Liu and Orfila's (2004) approach to quantify the viscous effects inside the bottom boundary layer for the case of channels with arbitrary cross-section. The viscous effects in the boundary layer induce mass fluxes into the core region where Boussinesq equations are solved. Thus, the cross-sectional averaged equation for conservation of mass is modified by adding the mass flux across the channel boundary, which has the form of a convolution integral.

For a straight channel with a slowly-varying cross-section, the continuity equation [9] becomes

$$\begin{aligned}\frac{\partial\tilde{\eta}}{\partial t}+\varepsilon\frac{B'_0}{B_0}\tilde{\eta}\frac{\partial}{\partial x}(A_0\langle u\rangle)+\frac{1}{B_0}\frac{\partial}{\partial x}([A_0+\varepsilon B_0\tilde{\eta}]\langle u\rangle)\\ -\frac{\delta}{\mu}\left(\frac{1+2h/B_0}{\sqrt{\pi}}\right)\int_0^t\frac{\partial\langle u(x,\tau)\rangle/\partial x}{\sqrt{t-\tau}}d\tau=O(\varepsilon^2,\varepsilon\mu^2,\mu^4)\end{aligned} \quad [11]$$

where $\delta^2=\hat{\nu}/\hat{\lambda}\left(\hat{g}\hat{h}_0\right)^{1/2}$ represents a dimensionless measure of viscous effects, with $\hat{\nu}=10^{-6}\,\mathrm{m}/s$ being the kinematic viscosity of water. Here, we assume $\delta=O(\varepsilon^2,\mu^4)$, so that the viscous effects are slightly weaker than the frequency dispersion and nonlinear effects, but not too small to be neglected. The cross-sectional averaged momentum equation remains unchanged. This analytical approach to quantify the viscous effects is solely appropriate for small-scale laboratory experiments where the boundary layer remains laminar. Other cases requiring the implementation of turbulent models or bottom friction are not covered herein.

4. JUCTIONS

Winckler (2015) derived compatibility conditions to solve for junctions in branching channels. To derive these conditions, the physical region is divided into a near and a far field according to the dominant scales in each region. This is essentially similar to the approach used by Mei et al. (2005) to solve the wave propagation on a straight depth discontinuity. The detailed derivation can be reviewed in Winckler (2015).

To a leading order error of $O(\mu)$, corresponding to a linear nondispersive wave theory, the compatibility conditions are very simple. Indeed, the equation of conservation of mass can be expressed as

$$\sum_{i=1}^{N_{in}} B_0^{(i)} \langle u_n \rangle^{(i)} - \sum_{i=1}^{N_{out}} B_0^{(i)} \langle u_n \rangle^{(i)} = O(\mu), \qquad [12]$$

where N_{in} and N_{out} corresponds to the number of inlets and outlets at the junction, $\langle u_n \rangle^{(i)}$ is the cross-sectional averaged longitudinal velocity normal to each cross-section and $B_0^{(i)}$ the surface width at the quiescent state on each branch. The conservation of momentum, on the other hand, is

$$\nabla \eta = O(\mu), \qquad [13]$$

Implying that $\tilde{\eta}$ has the same value for all branches at the junction. Thus, to the lowest order of approximation, conditions [12] and [13] imply that on the junction, the surface elevation is the same for the concurrent branches and the fluxes sum up to zero. This first order approximation loses detailed information on the wave features but retains the leading order effects on flow features. It also predicts that the angle of the branches is irrelevant for the flow properties across the junctions.

If i) the typical length scale of the junction is much smaller than the propagation distance, and ii) the wave amplitude is relatively small, then nonlinear and dispersive effects may be assumed negligible in the vicinity of the junction. Under these conditions, compatibility conditions [12] and [13] can be used in conjunction with the Boussinesq-type equations derived in the earlier sections. Such scheme is useful for modeling long waves in channel networks.

5. APPLICATIONS

In this talk, the capability of the present set of modeling tools will be discussed by means of three examples, namely i) a solitary wave on a shoaling beach, ii) a solitary wave on a curved transition and iii) a solitary wave passing through a junction. The first example is explained in Winckler and Liu (2015), thus omitted herein, while the third is still under development. Only the second example is detailed herein.

The influence of curvature in the wave flow is explored by means of two channels with curved transitions. The so called concave-convex channel consists of an initial straight section followed by a concave transition between points A and M, a convex transition between points M and B and a final straight section (Figure 2a). In the convex-concave channel, the transition is reversed (Figure 2b).

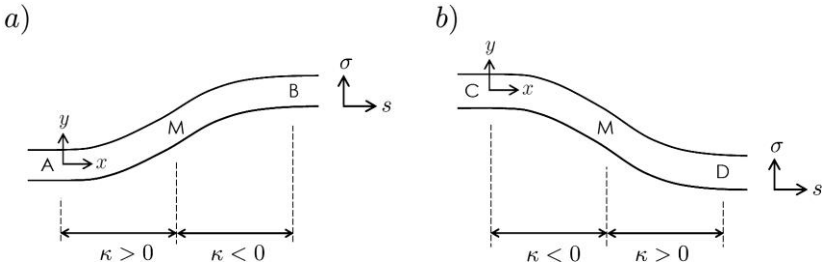

Figure 2. a) concave-convex channel b) convex-concave channel.

Rectangular uniform channels with a constant width of $B_0 = 1\ \mathrm{m}$ and a depth of $h = A_0/B_0 = 1\ \mathrm{m}$ are considered. The governing equations [4] and [8], in dimensional form (hats are omitted for dimensional variables), are reduced to

$$\left(1 - \kappa \frac{B_0}{2}\right) \frac{\partial \tilde{\eta}}{\partial t} + \frac{1}{B_0} \frac{\partial}{\partial s} ([A_0 + \varepsilon B_0 \tilde{\eta}] \langle u \rangle) = 0 \qquad [14]$$

and

$$\left(1 - \kappa \frac{B_0}{2}\right) \frac{\partial \langle u \rangle}{\partial t} + g \frac{\partial \tilde{\eta}}{\partial s} + \langle u \rangle \frac{\partial \langle u \rangle}{\partial s} + \gamma \frac{\partial^3 \langle u \rangle}{\partial t \partial s^2} = 0, \qquad [15]$$

where the terms containing $\alpha, \beta, \vartheta, \Gamma = 0$ due to the uniform cross-section, and $\sigma_c = B_0/2$. These equations are solved numerically by using the fourth order Adams-Bashforth-Moulton method (Wei and Kirby 1995). An incoming wave with amplitude $a_0 = 0.15\ \mathrm{m}$ m and a typical wavelength of $\lambda_0 = O(5\ \mathrm{m})$ is considered. Nonlinearity and frequency dispersion are characterized by $\varepsilon = a_0/h = O(0.1)$ and $\mu = h/\lambda_0 = O(0.2)$, thus the Boussinesq approximation is fulfilled. The geometry is defined in local $x - y$ coordinates with an origin at the beginning of the transitions (i.e. points A and C in Figure 2).

The transition for the channel in Figure 2a has a sinusoidal shape of the form

$$y = \begin{cases} 0 & x \le 0 \\ A + Asin(K_t x - \pi/2) & 0 < x \le \pi/K_t \\ 2A & \pi/K_t < x \end{cases} \quad [16]$$

where A and K_t are chosen to satisfy the assumption $B_0 \ll \lambda_0 \ll R_0$. Specifically, $A = 100\ \mathrm{m}$ and $K_t = 2\pi/200 = 0.0314\mathrm{m}^{-1}$. The curvature is given by

$$\kappa(x,y) = \frac{y_{xx}}{[1+(y_x)^2]^{3/2}}. \quad [17]$$

To map the curvature into the curvilinear coordinate system, $\kappa(s)$, the arc length is defined by

$$s(x,y) = \int_0^s ds = \int_0^x \sqrt{1+(y_x)^2}dx, \quad [18]$$

which is an elliptic integral of the second kind with no analytic solution, and is solved through numerical integration. The curvature as a function of the s coordinate is depicted in Figure 3a. Note that the transition begins at $s = 50$ m, whereas the in local coordinates, it starts at $x = 0$ m.

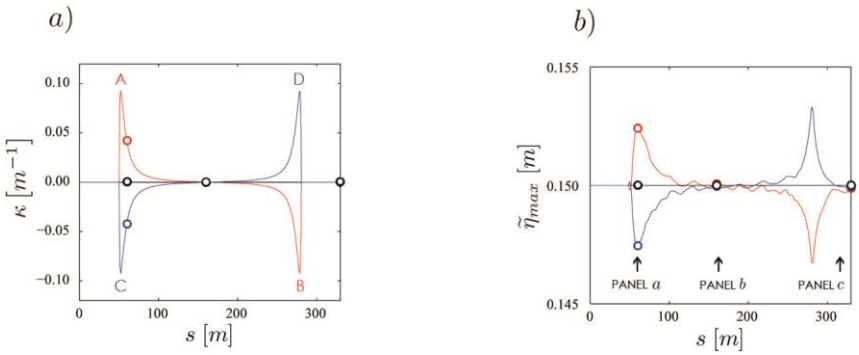

Figure 3. a) Curvature along a concave-convex channel (red), a straight channel (black) and a convex-concave channel (blue). b) maximum amplitude at each point during the simulation. Relevant points in Figure 2 are included.

The maximum amplitude at each point during the simulation is depicted in Figure 3b. It is observed that the point where the curvature effect on surface elevation is more pronounced ($s = 60$ m) occurs downstream from the point with maximum curvature ($x = 50$ m). This implies that the effect of curvature is delayed as a consequence of the second order terms in the governing equations. Downstream of the transition ($s > 300$ m), the maximum amplitude for all channels converges to that of the initiation, implying that the curvature effects are reversible.

Figure 4 shows surface profiles a) between the start and the midpoint of the transition where the curvature effect is more pronounced, b) near the midpoint and c) after the transition's end. Panel a) shows that waves in the concave-convex channel have propagated only through the concave section with a slight increase of the wave amplitude and phase speed (with respect to the straight channel). For the convex-concave channel, on the other hand, waves have traveled through the convex section and the effects are opposite in magnitude as a consequence of the change of sign in the curvature. These small differences in wave amplitude between cases are explained due to the fact that waves have traveled only about two wavelengths along the transition, so cumulative effects due to curvature are small. Panel b) shows that near the middle of the transition, the amplitude is almost equal in all channels but the position of the peak is slightly downstream for the concave-convex channel ($s = 160.2$ m) than for the convex channel ($s = 158.9$ m), as a consequence of the different phase speeds in both cases. Panel c) shows that the main waves have almost recovered the original form at the transition's end for all cases, with only slight differences in the trailing waves.

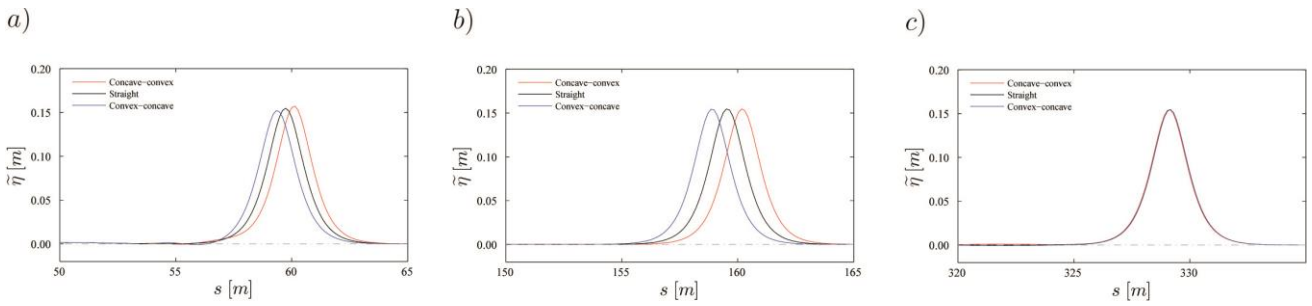

Figure 4. Surface profiles for a concave-convex channel (red), a straight channel (black) and a convex-concave channel (blue). Results a) where the curvature effect is more pronounced, b) at the center and c) at the end of the transition.

It is concluded that i) the solution for the wave field in a uniform rectangular channel with curvature in the horizontal plane is locally affected by the magnitude and sign of the curvature, ii) curvature effects are reversible in channels that recover the alignment after a sinusoidal transition and that iii) cumulative effects of curvature, such as the generation of trailing waves, appear to be minor. The generalization of all or some of these features to non-symmetric transitions or channels of non-symmetric cross-sections cannot be done at this stage.

The theory for curved channels is under development and has still some issued to be resolved (Winckler, 2015). For example, to the order of approximation used, the perturbation solution does not capture the free surface tilting due to curvature; however, the fact that the coordinate system traces the channel is indeed an implicit inclusion of the curvature. The solution for the cross-sectional averaged quantities, on the other hand, depends on the position of the coordinate system used (e.g. left sidewall, center of right sidewall). This result, though counterintuitive, can be explained due to the fact that the unknown quantities, $\tilde{\eta}$ and $\langle u \rangle$, do not represent the same cross-section (see Winckler, 2015 for a deeper explanation).

6. CONCLUSIONS

A set of tools intended to improve the physical understanding of long wave propagation in channels is presented in this talk. A new theory for weakly-nonlinear weakly-dispersive waves in curved channels based on a curvilinear orthogonal system is first derived. This theory is a generalization of the theory for a straight channels by Winckler and Liu (2015), and accounts for arbitrary cross-sections that can change appreciatively within a wavelength. Compatibility conditions for junctions are also derived for linear nondispersive waves. Under the assumptions that junctions are relatively small compared to the wavelength and that waves are small, these conditions can be combined with the new theory for curved channels to model wave propagation in complex network systems. Finally, the inclusion of viscous effects stemming from the bottom boundary layer is useful to characterize long wave patterns in small scale experiments.

The new set of tools can be used in a variety of problems. As an example, for landslide tsunami in fjords, travel-times and maximum wave heights can be rapidly estimated from 1D governing equations, making these tools suitable for warning systems. Other applications are river dynamics, flood and tidal waves in estuaries, among other phenomena.

ACKNOWLEDGMENTS

The research is supported by NSF grants to Cornell University. P. Winckler would also like to thank Fulbright, CONICYT and Universidad de Valparaíso for financial assistance in the form of a studentship.

REFERENCES

Dressler, R. F. (1978). New nonlinear shallow-flow equations with curvature. *Journal of Hydraulic Research*, 16(3):205-222.

Fenton J.D. and Nalder, G.V. (1995) . Long wave equations for waterways curved in plan. In 26th Congress of the International Association for Hydraulic Research, London. International Association for Hydraulic Research, 11-15 September 1995.

Mei, C.C.; Stiassnie, M. and Yue, D. K.-P. (2005). Theory and applications of ocean surface waves. Part 2: Nonlinear aspects, volume 23 of Advanced Series on Ocean Engineering. World Scientific.

Nachbin, A. and DaSilva, V. (2012). Solitary waves in open channels with abrupt turns and branching points. *Journal of Nonlinear Mathematical Physics*, 19:1-21.

Peregrine, D.H. (1968). Long waves in a uniform channel of arbitrary cross-section. *Journal of Fluid Mechanics*, 32:353-365.

Teng, M. and Wu, T. (1997). Effect of cross-sectional geometry on long wave generation and propagation. *Physics of Fluids*, 9(11):1-10.

Wei, G. and Kirby, J. T. (1995). Time dependent numerical code for extended boussinesq equations. *Journal of Waterway, Port, Coastal and Ocean Engineering*. ASCE, 121(5):251-261.

Winckler, P. (2015). Long waves in channels of non-uniform cross-section. PhD. dissertation, School of Civil and Environmental Engineering, Cornell University.

Winckler, P. and Liu, P. L. F. (2015). Long waves in a straight channel with non-uniform cross-section. *Journal of Fluid Mechanics*, accepted.